RSC Advances

PAPER

Cite this: *RSC Adv.*, 2016, **6**, 34903

Evolution of morphologies of a PE-*b*-PEO block copolymer in an epoxy solvent induced by polymerization followed by crystallization-driven self-assembly of PE blocks during cooling

Julieta Puig,[a] Ileana A. Zucchi,*[a] Marcelo Ceolín,[b] Walter F. Schroeder[a] and Roberto J. J. Williams[a]

Received 1st February 2016
Accepted 29th March 2016

DOI: 10.1039/c6ra03019j

www.rsc.org/advances

Polymerization-induced nanostructuration combined with crystallization-driven self-assembly was used to generate complex nanostructures in an epoxy network. A PE-*b*-PEO block copolymer ($M_n = 1400$; 50 wt% PEO), was dispersed in diglycidylether of bisphenol A (DGEBA) and homopolymerization initiated by a tertiary amine was carried out at 120 °C (above the melting temperature of PE). The plasticization produced by the miscible PEO blocks decreased the T_g of the cured matrix to values located below the crystallization temperature of PE. Therefore, crystallization-driven self-assembly of PE blocks took place during the cooling step through the rubbery region of the epoxy network. Depending on the initial amount of PE-*b*-PEO dispersed in DGEBA, a variety of nanostructures could be generated, such as a dispersion of disk-like micelles (6.7 nm in thickness), a concentrated dispersion of short nanoribbons (50–200 nm in length and 6.7 nm in thickness), partially stacked and oriented in space, and complex spherulitic structures composed of large stacked nanoribbons. The thickness of micellar objects was close to the theoretical value of fully extended PE chains of the block copolymer. IR spectroscopy confirmed the *all-trans* conformation of PE chains. Therefore, crystals were formed by interdigitated PE chains, with PEO blocks tethered at both planar interfaces in an alternating way. The way in which these complex nanostructures affect the fracture resistance or functional properties (such as shape memory) of the resulting epoxy networks has yet to be analyzed.

1. Introduction

Since the seminal studies reporting the nanostructuration of block copolymers in polymer networks,[1,2] a large number of papers and reviews[3] describing the generation of micellar or ordered structures (cubic, cylindrical, gyroid, lamellar), in polymer networks, have been published. Focus has been placed on nanostructures that are convenient for toughening purposes,[3–11] for processing aids,[12,13] or for developing specific functional properties.[14–17]

The nanostructuration of the block copolymer in the polymer network requires an immiscible block, either initially or during polymerization,[18,19] and another block that keeps its miscibility up to high conversions. The latter is a necessary condition to avoid macrophase separation. The nanostructures initially generated can evolve during polymerization due to the change of the quality of the reactive solvent with respect to the miscible block.[2,20] It varies from a good to a poor solvent due to the decrease in the entropic contribution to the free energy of mixing in the pregel stage and the appearance of an elastic energy contribution in the postgel stage.[21] Besides, the fraction of reactive solvent that is partitioned with the immiscible block can vary during polymerization, leading also to changes in the nanostructure.[22] Cure cycles can be selected to convey the evolution of morphologies to desired nanostructures in the final material.[20]

When the immiscible block is crystallizable, a different set of nanostructures can be generated, depending on the selection of the cure cycle. When the polymerization is performed *below* the crystallization temperature of the immiscible block, the initial blend consists of a dispersion of crystalline nanostructures stabilized by the miscible block. Zucchi and Schroeder[23] used a polyethylene (PE)–poly(ethylene oxide) (PEO) block copolymer, PE-*b*-PEO ($M_n = 1400$; 50 wt% PEO), dissolved in diglycidyl ether of bisphenol A (DGEBA). PEO is the miscible block while PE is the crystallizable one. At room temperature, a lamellar aggregation of large crystalline nanoribbons, dispersed in the reactive solvent, was observed. The

[a]*Institute of Materials Science and Technology (INTEMA), University of Mar del Plata and National Research Council (CONICET), J. B. Justo 4302, 7600 Mar del Plata, Argentina. E-mail: ileanazu@yahoo.com.ar; Fax: +54-223-481-0046; Tel: +54-223-481-6600*

[b]*Instituto de Investigaciones Físicoquímicas Teóricas y Aplicadas (INIFTA), Universidad Nacional de La Plata, CONICET, CC 16-Suc. 4, La Plata, Argentina*

photoinitiated cationic polymerization of DGEBA, performed at room temperature (below the melting temperature of PE), fixed the main structure and increased the interlamellar distance. When the polymerization is performed *above* the melting temperature of the PE block, crystallization takes place during the final cooling step.[14,24–26]

Guo *et al.*[24] were the first authors to analyze the nanostructuration occurring when polymerization is carried out above the melting temperature of the crystallizable block. They employed PE-*b*-PEO (M_n = 1400; 50 wt% PEO), dispersed in a stoichiometric solution of DGEBA and 4,4′-methylenedianiline (MDA). The cure cycle was performed in steps from 120 °C to 180 °C (above the melting temperature of PE). For block copolymer contents up to 30 wt%, the final materials were transparent after cooling to room temperature. PE was present as spherical micelles with a diameter close to 10 nm. Confined crystallization took place by homogeneous nucleation in the spherical micelles (minimum of the exothermic peak at 56 °C in DSC scans). Melting occurred at 96 °C (maximum of the endothermic peak in DSC scans). Tercjak *et al.*[14] employed PE-*b*-PEO (M_n = 920; 50 wt% PEO), dispersed in a stoichiometric solution of DGEBA and 4,4′-methylenebis(3-chloro-2,6-diethylaniline) (MCDEA). The cure cycle was performed in steps from 120 °C to 200 °C. The thermo-optical reversibility (transparent to opaque transition) of cured blends containing 40 wt% block copolymer was investigated. Yi *et al.*[25] employed the same block copolymer and thermoset precursors than Guo *et al.*[24] and re-analyzed the confined crystallization of PE in the nanostructures generated. Zhang and Zheng[26] synthesized a triblock copolymer, PCL-*b*-PE-*b*-PCL (M_n = 31 000 with 35 wt% PE), where poly(ε-caprolactone) (PCL) was the miscible block. It was dispersed in a stoichiometric solution of DGEBA and 4,4′-methylenebis(2-chloroaniline) (MOCA). The cure cycle was performed in two steps, at 150 and 180 °C. Cured blends containing up to 40 wt% block copolymer were nanostructured as a dispersion of spherical micelles. Diameters increased from 38 nm (10 wt% block copolymer) to 68 nm (40 wt% block copolymer). Confined crystallization of PE in these nanodomains was analyzed. It occurred at about 75 °C (minimum of the exothermic peak in DSC scans); melting was observed at 120–125 °C (maximum of the endothermic peak in DSC scans).

In all these previous studies, high-T_g (glass transition temperature) epoxy networks were selected. In spite of the plasticization effect produced by the miscible block, the resulting T_g's were still higher than the crystallization temperature of PE. Therefore, when cooling from the reaction temperature, vitrification of the epoxy matrix took place before crystallization of PE. This fixed the nanostructure generated at high temperatures and enabled crystallization to occur in confined domains with rigid boundaries. A different situation could occur when the T_g of the epoxy network is lower than the crystallization temperature of PE. In this case, a crystallization-driven self-assembly[27] of PE nanodomains generated at the polymerization temperature, may take place during cooling in the temperature gap comprised between the crystallization temperature and the glass transition of the matrix. The crystal packing forces can produce the self-assembly of cores into nanostructures that cannot be accessed by other strategies. This is the focus of the present study.

We selected PE-*b*-PEO (M_n = 1400; 50 wt% PEO), dispersed in DGEBA that was homopolymerized by an anionic mechanism using a tertiary amine as initiator. The reaction was carried out at 120 °C (above the melting temperature of PE). Two different amines were selected: benzyldimethylamine (BDMA) and 4-dimethylamino(pyridine) (DMAP). BDMA gave a relatively slow rate of polymerization enabling to follow the nanostructuration in the course of reaction. DMAP produced a much faster rate[28] and was employed to analyze the effect of a fast reaction on nanostructures generated. The plasticization produced by the miscible PEO blocks decreased the T_g of the matrix to values located below the crystallization temperature of PE. Therefore, crystallization-driven self-assembly of PE blocks took place during the cooling step.

2. Experimental section

2.1. Materials

The epoxy monomer was based on diglycidyl ether of bisphenol A (DGEBA, DER 332 Aldrich) with an epoxy equivalent weight of 174.3 g per eq., corresponding to 0.015 hydroxyls per epoxy group. Two different tertiary amines were selected as initiators of the anionic homopolymerization of DGEBA: benzyldimethylamine (BDMA, ≥99%, Aldrich) and 4-dimethylamino(pyridine) (DMAP, ≥98%, Fluka). The block copolymer was PE-*b*-PEO (M_n = 1400; 50 wt% PEO, Aldrich). Chemical structures of these materials are shown in Fig. 1.

2.2. Synthesis of epoxy networks modified by PE-*b*-PEO

Blends containing 10, 20 or 40 wt% PE-*b*-PEO in DGEBA, were placed in a vial and purged with nitrogen for 30 min at room temperature. The vial was then placed in an oil bath kept at 150 °C while stirring continuously to produce the homogeneous dispersion of the block copolymer. After cooling to room temperature, the selected tertiary amine was added in a molar ratio with respect to epoxy groups equal to 0.06 for BDMA[29,30] or 0.08 for DMAP.[28] Most of the results were obtained using BDMA. DMAP was only used to assess the effect of a fast reaction rate. Then, the blend was heated to 100 °C, stirred for about 1 min and transferred to the device used for characterization or cast over an aluminum substrate (film of about 1 mm thickness). Cure was performed in an oven under a nitrogen atmosphere, at 120 °C for 3 h.

2.3. Characterization techniques

Near-infrared spectroscopy (FT-NIR) and middle-infrared spectroscopy (FT-MIR) were used to follow the conversion of epoxy groups and to monitor the presence and evolution of specific bands. Measurements were conducted on a Nicolet 6700 Thermo Scientific IR device provided with a heated transmission cell (HT-32, Spectra Tech) and a temperature controller (CAL 9500P, Spectra Tech). Near-infrared (NIR) spectra were acquired over the 4000–7000 cm^{-1} range, from 32 co-added scans at 4 cm^{-1} resolution. Samples were placed between

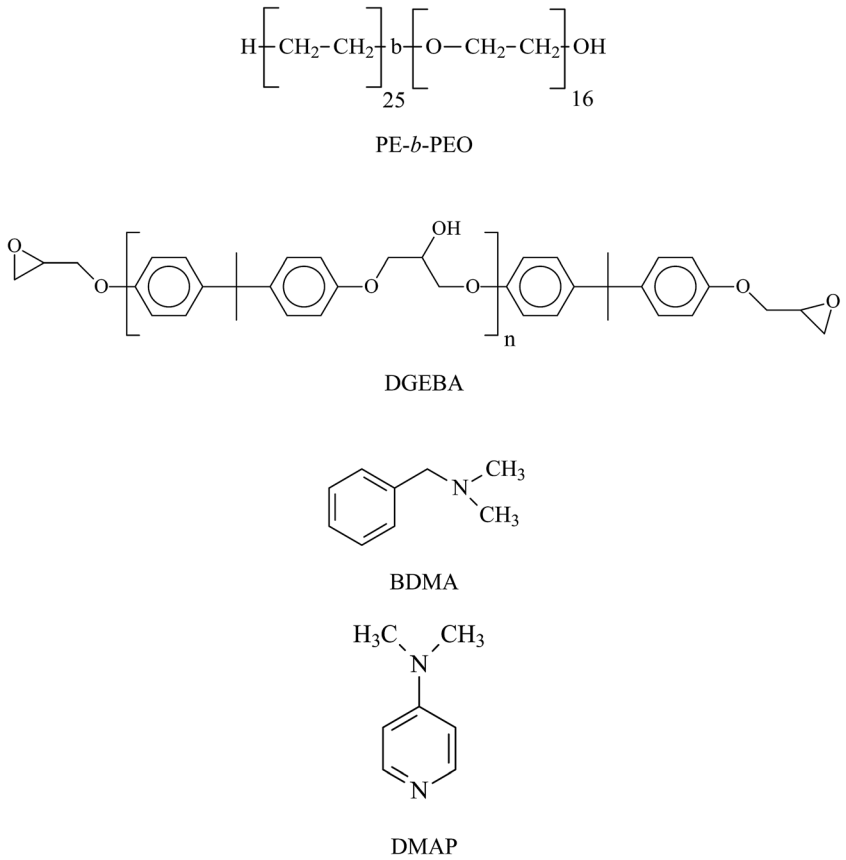

Fig. 1 Chemical structures of the different materials.

glass windows using a rubber spacer of 1.4 mm. MIR measurements were performed placing the sample between KBr windows using a rubber spacer of 200 μm. Spectra of cured blends were obtained in the attenuated total reflectance mode (smart Orbit ATR accessory).

Thermal characterization of different blends was performed by differential scanning calorimetry under a dry nitrogen atmosphere (DSC, Perkin-Elmer Pyris 1). Samples (about 10 mg in weight) were first heated from −50 °C to 190 °C, at 10 °C min^{-1}, and subsequently cooled to −50 °C at the same rate to detect crystallization. Glass transition temperatures were defined at the onset value of the change in the specific heat during the heating scans.

Optical properties of blends polymerized at 120 °C between two glass covers and then cooled to room temperature at 10 °C min^{-1}, were determined by transmission optical microscopy (TOM). A Leica DMLB microscope provided with a hot stage (Linkman THMS 600) was employed.

The evolution of the storage (G') and loss modulus (G'') along reaction at 120 °C, was followed using an Anton Paar rheometer (model Physica MCR-301) provided with a CTD thermo chamber. A parallel-plate configuration (diameter $D = 25$ mm, gap $H = 0.5$ mm) was used in oscillatory mode at 1 Hz with a 10% amplitude.

Small-angle X-ray scattering (SAXS) experiments were performed *in situ* during the cure at 120 °C and the subsequent cooling to room temperature at 10 °C min^{-1}. The SAXS system (INIFTA, project "Nanopymes", EuropeAid/132184/D/SUP/AR-Contract 331-896) is a XEUSS 1.0 HR (XENOCS, Grenoble) equipped with a microfocus X-ray source and a Pilatus 100K detector (Dectris, Switzerland). The temperature of the samples was controlled using a HFSX350 device within ±0.1 K (Linkam Scientific Instruments, UK). SAXS diagrams of cured blends were also recorded at room temperature in the small-angle X-ray scattering station (beamline SAXS 1) of the National Laboratory of Synchrotron Light (LNLS, Campinas, Brazil). For *in situ* measurements, samples were placed inside quartz glass capillaries with an external diameter of 1.5 mm and a thickness of 0.01 mm (WJM-Glas/Müller GmbH). The capillary was fixed inside the beam using a holder so that all data were recorded at the same position with an acquisition time of 15 min. The scattering intensity (in arbitrary units) was recorded as a function of the scattering vector $q = (4\pi/\lambda)\sin\theta$, where λ is the radiation wavelength (1.5419 Å) and 2θ the scattering angle. Scattering profiles were analyzed using SASfit software package.

Transmission electron microscopy (TEM) images were obtained for cured samples at room temperature using a JEOL 100CX electron microscope operated at an accelerating voltage of 80 kV. Cured samples were microtomed at room temperature with an LKB ultramicrotome equipped with a diamond knife. The ultrathin sections (*ca.* 60 nm in thickness) were collected on copper grids. Enough contrast of different phases was observed

without any staining procedure.[23] However, one of the samples was stained with RuO_4 to enhance contrast between phases. RuO_4 selectively stains the components in the following order (most stained to least stained): PEO > epoxy > PE.[2]

3. Results and discussion

3.1. Evolution of PEO miscibility during reaction

The anionic homopolymerization of DGEBA is initiated by tertiary amines and catalyzed by OH groups.[28,29,31,32] Hydroxyl groups are initially present in the chemical structures of DGEBA and the block copolymer (Fig. 1), and are continuously produced by termination reactions generating OH and vinylidene groups,[28] as shown in Fig. 2. Therefore, the reaction follows an autocatalytic mechanism. The miscibility of PEO blocks is improved during polymerization due to two factors: (a) increase in H-bonds among ether and OH groups;[20] (b) covalent bonding by proton abstraction of OH terminal groups of PEO by the propagating alkoxide anions.[28] Simultaneously, the continuous increase in the size of epoxy oligomers decreases the miscibility of PEO through the decrease in the entropic contribution to the free energy of mixing. These opposing effects affect the quality of the reactive solvent with respect to PEO blocks. As will be discussed later, the solvent becomes better at low conversions and worst at high conversions (but still a solvent), as revealed by the evolution of the nanostructures generated.

3.2. Blend with 10 wt% PE-*b*-PEO

In the first place, we analyzed the thermal properties of the fully cured blend to assess that the glass transition temperature of the epoxy matrix plasticized by PEO was lower than the crystallization temperature of PE. Fig. 3 shows DSC scans obtained in heating and cooling cycles at 10 °C min^{-1}.

The heating cycle shows the T_g of the plasticized epoxy at 58 °C (onset value), that was significantly lower than the value of the neat epoxy (81 °C, not shown). After the glass transition, there was no residual exothermic peak of reaction implying that the reaction was completed with the selected cure cycle. PE crystals melted at 98 °C (minimum of the endothermic peak). The cooling scan shows a crystallization peak at 65 °C. Therefore, this blend exhibits a very narrow temperature gap, from about 70 °C (onset of crystallization) to 58 °C, to produce a crystallization-driven self-assembly.

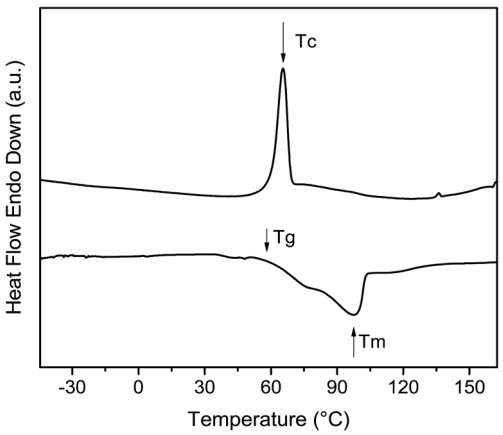

Fig. 3 DSC thermograms for the cured blend with 10 wt% PE-*b*-PEO in heating and cooling cycles at 10 °C min^{-1}.

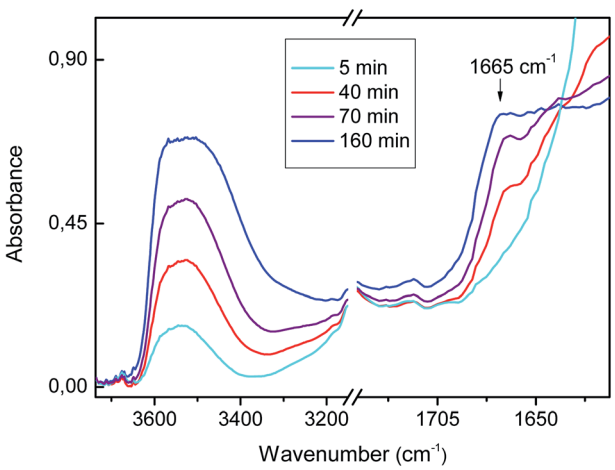

Fig. 2 Evolution of bands characteristic of OH groups (3400–3600 cm^{-1}) and vinylidene groups (1665 cm^{-1}) in IR spectra, for a blend containing 20 wt% PE-*b*-PEO during a BDMA-initiated polymerization at 120 °C.

Then, the optical transparency of the blend was observed by TOM. Unexpectedly, the unreacted blend at 120 °C was not fully transparent. Large structures with diffuse boundaries were present in the whole sample. However, after about 30 min reaction the blend became fully transparent and kept its transparency after 3 h at 120 °C where full conversion was reached. It may be inferred that the coarsened structure was disintegrated into a micellar structure during polymerization. This could be associated with the initial increase in the miscibility of PEO and epoxy species as explained in the previous section. Initially, the fraction of H-bonds between PEO and OH groups of DGEBA is very low and cannot counterbalance the association of the immiscible PE blocks that produces the coarsened structure. As conversion advances, there is a significant increase in the solubility of PEO. This is promoted by the increase in the concentration of OH groups produced in termination steps (Fig. 2), and by the covalent bonding of PEO blocks by transfer reactions to the propagating alkoxide anions. The blend remained transparent during cooling to room temperature meaning that crystallization did not produce any coarsening of the nanostructure generated at 120 °C.

The conversion of epoxy groups was followed by NIR spectroscopy, measuring the relative heights of the absorption band of epoxy groups at 4530 cm^{-1} with respect to a reference band located at 4620 cm^{-1}.[33] Fig. 4 shows conversion *vs.* time curves for the neat epoxy and for the blend with 10 wt% PE-*b*-PEO, along polymerization at 120 °C.

At low conversions, both curves are undistinguishable. However, after about 20 min, the blend with 10 wt% PE-*b*-PEO polymerized at a faster rate than the neat epoxy. A possible explanation is related to the increase of the exposure of terminal OH groups of PEO to epoxy species produced by the

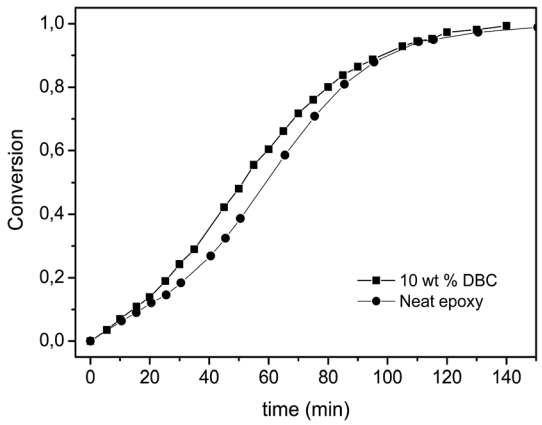

Fig. 4 Conversion *vs.* time curves for the neat epoxy and for the blend with 10 wt% PE-*b*-PEO, during polymerization at 120 °C.

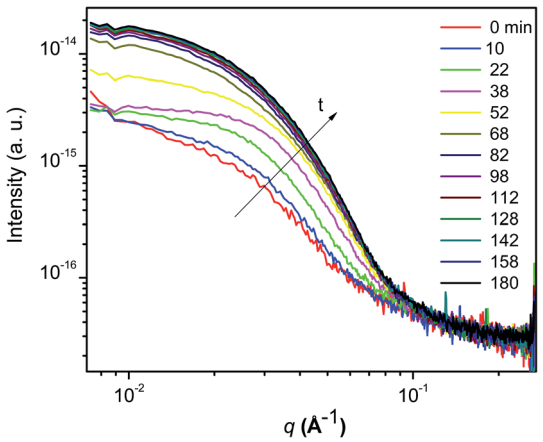

Fig. 6 *In situ* SAXS diagrams obtained during polymerization of the 10 wt% PE-*b*-PEO/epoxy blend at 120 °C.

transformation of the coarsened structure into a micellar dispersion during the first 30 min of reaction. The OH groups have a catalytic effect on the anionic homopolymerization as explained in the previous section.

Further information of the micellization process was obtained from rheological measurements. Fig. 5 shows the evolution of storage (G') and loss (G'') moduli of the blend with 10 wt% PE-*b*-PEO during polymerization at 120 °C.

At low reaction times, $G' > G''$ meaning that the blend behaved as a physical gel at 120 °C. This can be explained by percolation of the coarsened structure throughout the material. At about 12 min, there was a crossover of both moduli implying that the blend exhibited a liquid behavior produced by the ongoing transformation of the coarsened structure into a micellar dispersion. At about 34 min, a new crossover between both moduli was observed, corresponding to gelation of the epoxy matrix.

Fig. 6 shows *in situ* SAXS diagrams obtained during polymerization of the 10 wt% PE-*b*-PEO/epoxy blend at 120 °C (the curves were vertically shifted for the sake of clarity). From about 68 min reaction to 3 h, diagrams did not vary significantly.

SAXS results were analyzed using SASfit software package, in the region 0.08 to 0.5 nm^{-1} where the contribution of the neat matrix showed a negligible intensity. Data obtained at 0 and 10 min were modeled assuming the simultaneous presence of large polydisperse spheres and monodisperse spherical micelles (diameter d_{sph}). Data obtained at 22, 38 and 52 min were analyzed assuming only a population of polydisperse spherical micelles (d_{sph} close to 13 nm), meaning that the micellization process was almost completed at 22 min reaction. Within the uncertainties to compare reaction times obtained in different devices, this agrees with the disintegration of the physical gel and the translucent to transparent transition observed by optical microscopy. The analysis of SAXS diagrams obtained at 68 and 180 min required a population of short cylinders (diameter $d_{cyl} = 10.5$ nm and length $L_{cyl} = 23$ nm). In every case, polydispersity was accounted using log normal distributions. As shown in Fig. 7, a very good fitting of the evolution of SAXS data was achieved.

Comparing the average volume of spherical micelles ($V_{sph} = 1150$ nm^3) with the average volume of cylindrical micelles ($V_{cyl} = 2000$ nm^3), it may be inferred that a coalescence process took

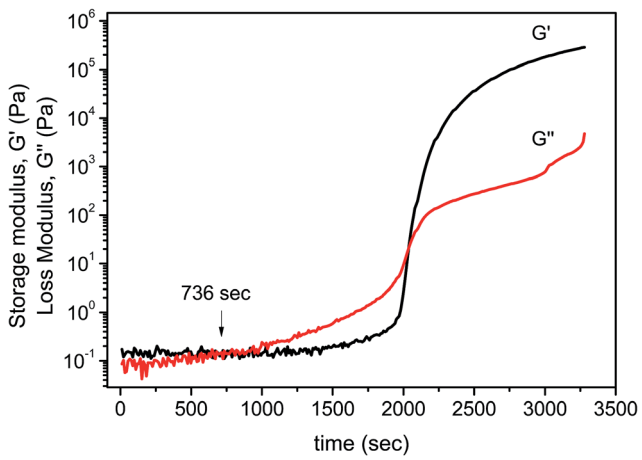

Fig. 5 Evolution of storage (G') and loss (G'') moduli of the blend with 10 wt% PE-*b*-PEO, during polymerization at 120 °C.

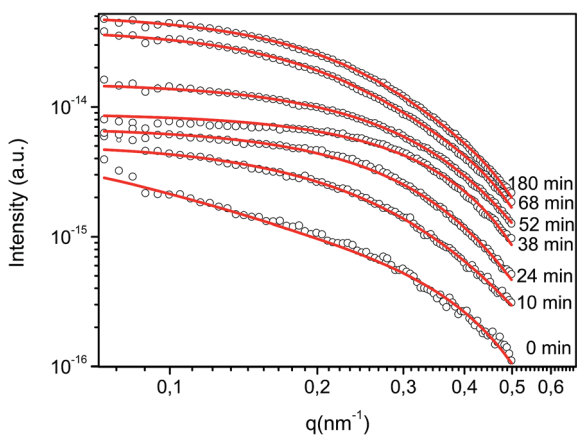

Fig. 7 Fitting of SAXS data obtained during polymerization of the 10 wt% PE-*b*-PEO/epoxy blend at 120 °C.

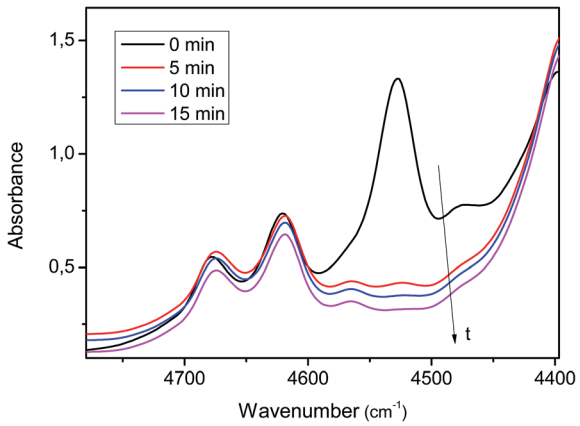

Fig. 8 Evolution of the epoxy peak at 4530 cm^{-1} in NIR spectra, during polymerization at 120 °C using DMAP as initiator.

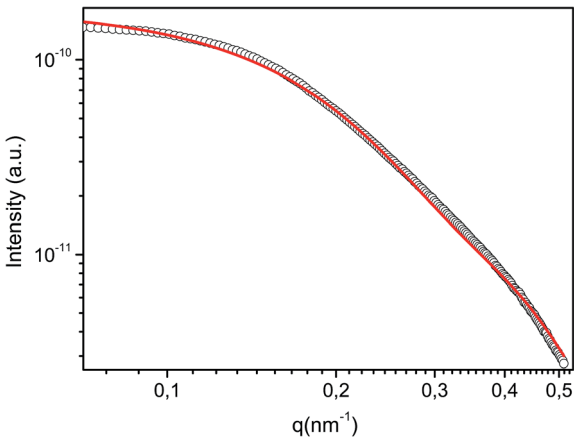

Fig. 10 Fitting of the SAXS diagram obtained after cooling the fully cured blend with 10 wt% PE-*b*-PEO to 30 °C.

place (about two spherical micelles generated one cylindrical micelle). The reason is the decrease in the solubility of PEO at advanced conversions, explained by thermodynamic reasons.[21] This produced both coalescence of micelles and a decrease of the interfacial curvature, from spheres to cylinders ("wet" to "dry" transition of PEO blocks).[2]

In order to get some more insight of the coarsened structure at 120 °C, BDMA was replaced by DMAP as initiator of the homopolymerization. Under these conditions, the reaction occurred at a very fast rate and initial morphologies could be kinetically trapped. Fig. 8 shows the evolution of the epoxy peak at 4530 cm^{-1} in NIR spectra, during polymerization at 120 °C. The reaction was almost completed after 5 min.

Fig. 9 shows a TEM image of the cured blend. Large domains with sizes in the range of 1–2 μm, are observed which are possibly some of the largest structures present in the initial population.

We then investigated if the crystallization-driven self-assembly of PE blocks produced any change in morphologies when cooling the BDMA-cured materials from 120 °C to room temperature at 10 °C min^{-1}. The narrow temperature gap where this process could take place was comprised between 70 °C (onset of crystallization) and 58 °C (end of vitrification in a cooling scan). Although the rate at which the cured blend traversed this temperature range could modify the extent of this process, this effect was not investigated (PE crystallizes at a very fast rate).

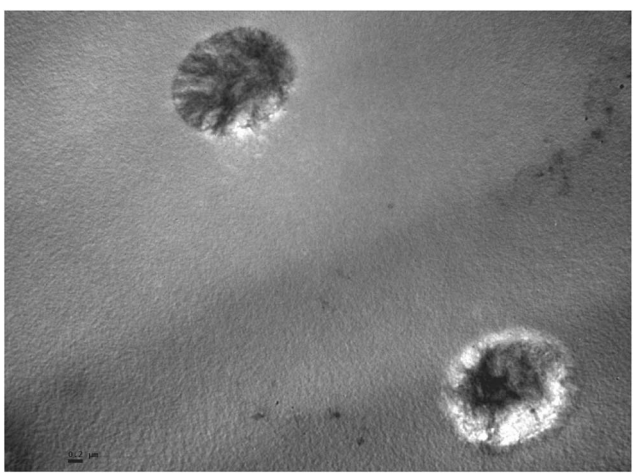

Fig. 9 TEM image of a 10 wt% PE-*b*-PEO/epoxy blend cured at 120 °C using DMAP as initiator.

Fig. 10 shows the fitting to SAXS diagram of the fully cured blend after cooling to 30 °C. The fitting required to assume the presence of a polydisperse distribution of planar objects (disk-like micelles) with an average diameter d_{disks} = 23.1 nm and a thickness h = 6.7 nm (V_{disks} = 2800 nm^3). The small increase of the volume of disks with respect to the starting cylindrical micelles might arise from the average dimensions taken from polydisperse distributions. Also, planar objects may have an ellipsoidal rather than a circular contour. Most probable, cooling led to a change of shape of individual micelles, from nanorods to disk-like objects, promoted by crystallization of PE chains. Fig. 11 shows a schematic representation of the evolution of morphology during cure and subsequent cooling to room temperature. This is completely different from the situation where vitrification of the epoxy matrix takes place before crystallization. In this case, the shape of the micelles generated at high temperatures is conserved and is not affected by the crystallization process in the confined domains.[24,26] It is interesting to point out that Yin and Hillmyer[34] also reported the formation of disk-like micelles when a solution of PE-*b*-poly(*N*,*N*-dimethylacrylamide) block copolymer in water was cooled to room temperature. In this case, spherical micelles present at high temperatures were transformed into disk-like micelles when cooling the solution to temperatures located below the crystallization temperature (maximum crystallization rate at 65 °C, the same one as in our case). It was also proved that no coalescence occurred during this process.

It is interesting to compare the thickness of the crystalline disk-like micelles with the one expected assuming that PE chains are fully extended. Methylene symmetric (d^+) and anti-symmetric peaks (d^-) for crystalline *n*-alkanes with fully extended chains in *all-trans* conformation, occur in the ranges

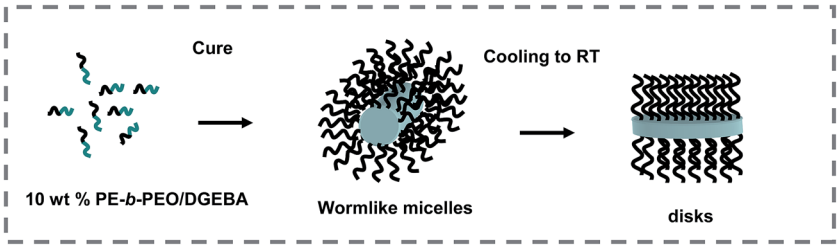

Fig. 11 Schematic description of the evolution of morphology of the sample containing 10 wt% PE-*b*-PEO during cure and subsequent cooling to RT.

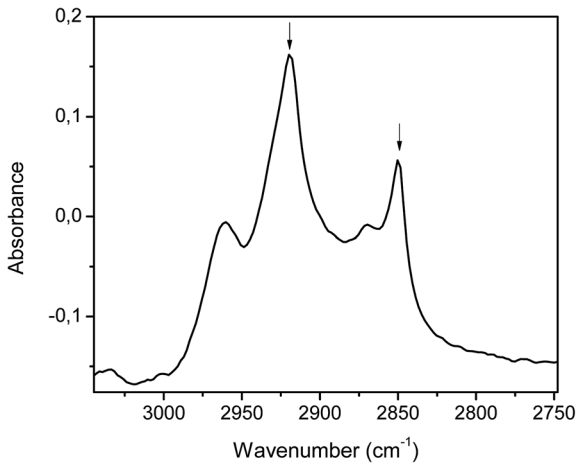

Fig. 12 IR spectrum in the methylene region of the fully cured blend containing 10 wt% PE-*b*-PEO, recorded at room temperature.

2846–2849 cm^{-1} and 2916–2918 cm^{-1}, respectively.[35] The increase in gauche population shifts these ranges to 2854–2856 cm^{-1} and 2924–2928 cm^{-1}.[36] Fig. 12 shows the IR spectrum in the methylene region of the fully cured blend containing 10 wt% PE-*b*-PEO, recorded at room temperature. Methylene bands were located at 2849 cm^{-1} and 2919 cm^{-1}, corresponding to fully extended PE chains. As every methylene group contributes with 0.1253 nm to the chain length,[37] and the block copolymer has 50 methylene units in the PE block, extended PE crystals must have a length of 6.27 nm, which is very close to the thickness of micellar disks (6.7 nm). Therefore, crystals are formed by interdigitated PE chains, with PEO blocks tethered at both planar interfaces in an alternating way. This configuration enables to accommodate PEO chains in space, a fact that could not be possible in a bilayer structure formed by tail to tail association of extended *n*-alkyl chains.

The presence of disk-like micelles with ellipsoidal contours was also observed in TEM images. Fig. 13 shows a representative image where a "face-on" disk-like micelle is enclosed by a circle and an "edge-on" disk-like micelle is pointed by an arrow (the thickness is close to the value obtained from SAXS data).

3.3. Blends with 20 and 40 wt% PE-*b*-PEO

The increase in the concentration of block copolymer produced significant changes in the evolution of morphologies. The first observation was that the initial coarsened structure present at 120 °C for the blend with 10 wt% PE-*b*-PEO, disintegrated more rapidly in the blend with 20 wt% block copolymer and was not present at all in the blend with 40 wt% PE-*b*-PEO. This means that the stability region of micelles in the initial epoxy solvent depends on the concentration of block copolymer. As in the case of dispersions of surfactants in water, there must exist a critical concentration (depending on temperature), above which the micellar dispersion is stable. Therefore, increasing the amount of block copolymer enabled the stabilization of a micellar structure in the initial solution at 120 °C. Correspondingly, physical gels were not formed in the initial blends containing 20 or 40 wt% PEO.

The second significant observation was that fully cured blends were transparent at 120 °C but became completely

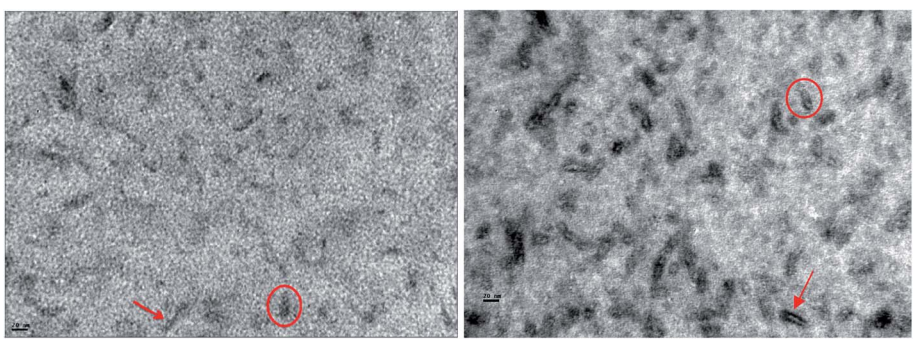

Fig. 13 TEM images of the fully cured blend containing 10 wt% PE-*b*-PEO. "Face-on" disk-like micelles are enclosed by a circle and "edge-on" disk-like micelles are pointed by an arrow. Left: Unstained sample. Right: Stained sample with RuO_4.

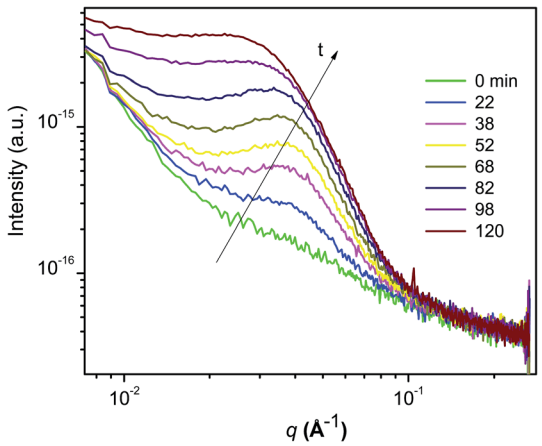

Fig. 14 *In situ* SAXS data obtained during polymerization of the 20 wt% PE-*b*-PEO/epoxy blend at 120 °C.

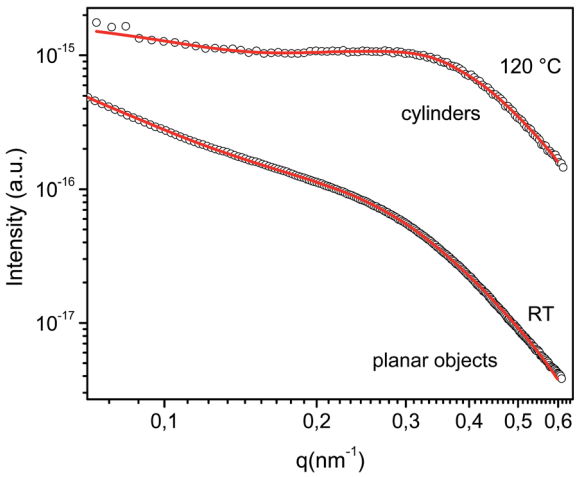

Fig. 15 Fitting of SAXS diagrams obtained from the fully cured blend at 120 °C and after cooling to room temperature.

opaque during the cooling stage, implying that a significant coalescence/stacking of individual micelles was driven by crystallization of PE blocks. This contrasts with the behavior of the fully cured blend with 10 wt% PE-*b*-PEO that remained transparent because crystallization was confined within individual micelles.

We will now analyze in more detail, the morphology generated in the blend with 20 wt% block copolymer. Fig. 14 shows *in situ* SAXS data obtained during polymerization of the 20 wt% PE-*b*-PEO/epoxy blend at 120 °C. In this case, the fitting was much more complex due to the need to introduce the structure factor accounting for the maximum observed in the spectra. This maximum is related to the average distance among nano-objects. From 22 min to 52 min it remained constant at about 17 nm ($2\pi/q_{max}$). At longer times the peaks shifted slightly to the left reflecting an increase in this characteristic distance. This can be ascribed to a partial coalescence of nanostructures that decreases their concentration and increases their separation. SAXS diagrams did not change after 98 min reaction (conversion close to 0.9).

Fig. 15 shows SAXS results obtained from fully cured blend at 120 °C and after cooling to room temperature. Crystallization of PE blocks produced a significant change in the shape of SAXS diagrams. While the one obtained at 120 °C could be modeled assuming the presence of cylindrical micelles ($d_{cyl} = 8.0$ nm, $L_{cyl} = 52.0$ nm), the fitting to the data obtained at room temperature required the presence of planar objects ($h = 6.7$ nm). As in the blend with 10 wt% PE-*b*-PEO, crystallization of PE blocks produced the flattening of cylindrical micelles. However, in the blend with 20 wt% block copolymer coarsening of the initial morphology took place as indicated by the loss of transparency of the blend.

The thickness of planar objects is the same as the one observed for the disk-like micelles generated in the blend with 10 wt% PE-*b*-PEO. It arises from the crystallization of PE blocks in *all trans* conformation, with amorphous PEO blocks tethered alternatively at both sides of the planar objects. The IR spectrum in the methylene region was similar to the one obtained for the blend with 10 wt% PE-*b*-PEO. Maxima were observed at 2849 cm^{-1} and 2916 cm^{-1}, characteristic of fully extended PE chains.

Fig. 16 shows a TEM image of the fully cured blend taken at room temperature. Planar nano-objects can be described as short nanoribbons with lengths ranging from about 50 to 200 nm. Partial coalescence of initial micelles by an end-to-end coupling process increased their length. Their partial stacking generated regions with short nanoribbons oriented in the same direction. This particular morphology could only be accessed by the crystallization-driven self-assembly process. Fig. 17 illustrates the evolution of the morphology during cure and posterior cooling to room temperature. If the blend is allowed to crystallize at room temperature before polymerization and is then photopolymerized at room temperature, large nanoribbons are generated (in the micrometer range) that are stacked into a lamellar structure.[23]

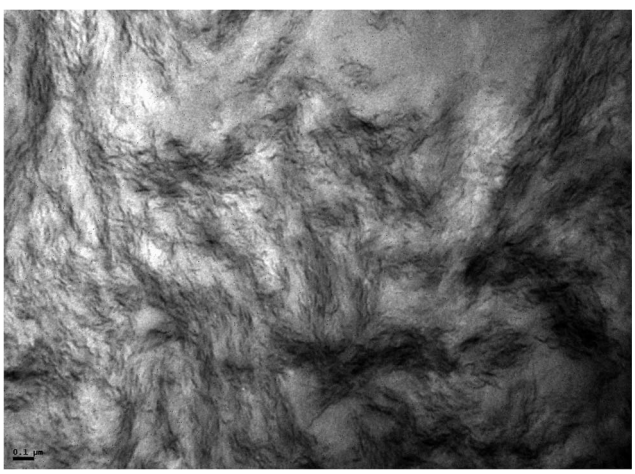

Fig. 16 TEM image taken at room temperature of the fully cured blend with 20 wt% PE-*b*-PEO.

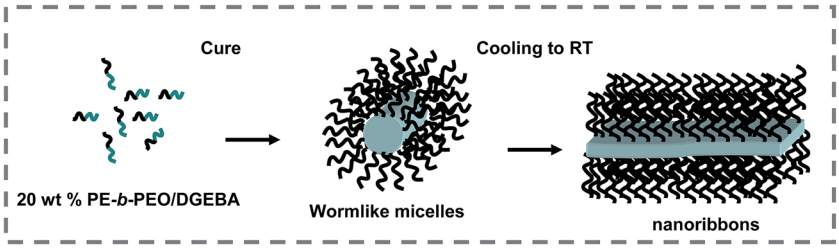

Fig. 17 Schematic description of the evolution of morphology of the sample containing 20 wt% PE-*b*-PEO during cure and subsequent cooling to RT.

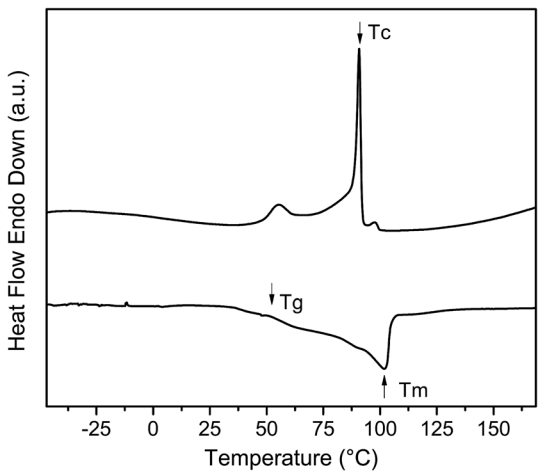

Fig. 18 DSC thermograms for the cured blend with 20 wt% PE-*b*-PEO in heating and cooling cycles at 10 °C min^{-1}.

Fig. 18 shows DSC scans obtained in heating and cooling cycles at 10 °C min^{-1} for the blend with 20 wt% block copolymer.

The heating cycle shows the T_g of the plasticized epoxy at about 52 °C (onset value) and the melting of PE crystals at 102 °C (minimum of the endothermic peak). The cooling cycle shows a strong crystallization peak at about 90 °C, characteristic of the crystallization of PE blocks in relatively large domains. The temperature range for crystallization-driven self-assembly in this blend extends from about 52 °C to 90 °C.

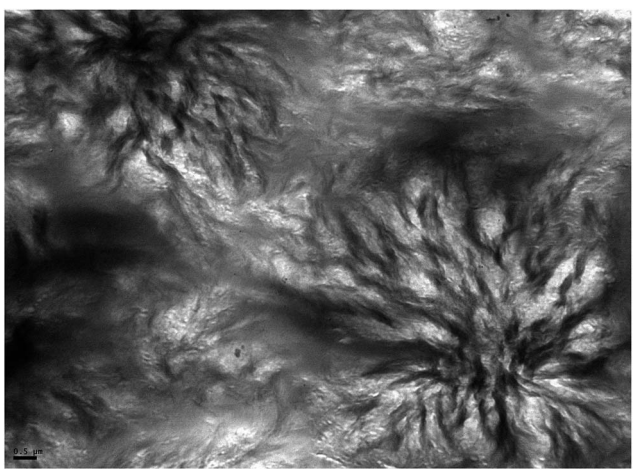

Fig. 19 TEM image taken at room temperature for the fully cured blend with 40 wt% PE-*b*-PEO.

Finally, Fig. 19 shows a TEM image taken at room temperature for the blend with 40 wt% PE-*b*-PEO. A large coarsening of the transparent micellar structure generated at 120 °C was produced when cooling to room temperature, driven by crystallization of PE blocks. Stacked nanoribbons of several μm in length are arranged into patterns typical of spherulitic growth. IR spectra in the methylene region showed maxima at 2847 cm^{-1} and 2915 cm^{-1}, characteristic of fully extended PE chains. This complex morphology was generated at a relatively fast rate in a crosslinked rubbery matrix during the cooling step from the polymerization temperature.

4. Conclusions

Polymerization-induced nanostructuration combined with crystallization-driven self-assembly was used to generate complex morphologies in an epoxy matrix. This required a block copolymer with a miscible block (PEO in the present study) and a crystallizable immiscible block (PE in this study), and epoxy precursors giving a glass transition temperature of the polymer network plasticized by the miscible block located below the crystallization temperature of the immiscible block. The polymerization was carried out at temperatures located above the melting temperature of crystals of the immiscible block, generating typical nanostructures (dispersion of cylindrical micelles in the present study). When cooling from the polymerization temperature, the cured blend traversed the temperature gap located between the crystallization temperature of immiscible blocks and the glass transition of the plasticized network. A new set of morphologies could be generated in this way by crystallization-driven self-assembly of the pre-existing nanostructures. This occurred in the rubbery region of the polymer network. In the present study, we showed that depending on the initial amount of PE-*b*-PEO dispersed in DGEBA, a variety of nanostructures could be generated, such as a dispersion of disk-like micelles (6.7 nm in thickness), a concentrated dispersion of short nanoribbons (50–200 nm in length and 6.7 nm in thickness), partially stacked and oriented in space, and complex spherulitic structures composed of large stacked nanoribbons. The way in which these complex

nanostructures affect fracture resistance or functional properties (such as shape memory) of the resulting epoxy networks has yet to be analyzed.

Acknowledgements

The financial support of the National Research Council (CONICET), the National Agency for the Promotion of Science and Technology (ANPCyT) and the University of Mar del Plata, is gratefully acknowledged. J. P. thanks Fundación Bunge y Born (Argentina) for a postdoctoral fellowship. SAXS experiments at INIFTA were performed thanks to project "Nanopymes" (EuropeAid/132184/D/SUP/AR-Contract 31-896). The grant SAXS1-17067 from the Brazilian Synchrotron Light Laboratory (LNLS, Campinas-SP, Brazil) is gratefully acknowledged.

References

1 M. A. Hillmyer, P. M. Lipic, D. A. Hajduk, K. Almdal and F. S. Bates, *J. Am. Chem. Soc.*, 1997, **119**, 2749.
2 P. M. Lipic, F. S. Bates and M. A. Hillmyer, *J. Am. Chem. Soc.*, 1998, **120**, 8963.
3 S. Zheng, in *Epoxy Polymers, New Materials and Innovations*, ed. J. P. Pascault and R. J. J. Williams, Wiley-VCH, Weinheim 2010, p. 81.
4 J. M. Dean, N. E. Verghese, H. Q. Pham and F. S. Bates, *Macromolecules*, 2003, **36**, 9267.
5 J. Wu, Y. S. Thio and F. S. Bates, *J. Polym. Sci., Part B: Polym. Phys.*, 2005, **43**, 1950.
6 Y. S. Thio, J. Wu and F. S. Bates, *Macromolecules*, 2006, **39**, 7187.
7 L. Ruiz-Pérez, G. J. Royston, J. P. A. Fairclough and A. J. Ryan, *Polymer*, 2008, **49**, 4475.
8 J. Liu, Z. J. Thompson, H. J. Sue, F. S. Bates, M. A. Hillmyer, M. Dettloff, G. Jacob, N. Verghese and H. Pham, *Macromolecules*, 2010, **43**, 7238.
9 C. Declet-Perez, E. M. Redline, L. F. Francis and F. S. Bates, *ACS Macro Lett.*, 2012, **1**, 338.
10 E. M. Redline, C. Declet-Perez, F. S. Bates and L. F. Francis, *Polymer*, 2014, **55**, 4172.
11 C. Declet-Perez, L. F. Francis and F. S. Bates, *Macromolecules*, 2015, **48**, 3672.
12 E. Girard-Reydet, J. P. Pascault, A. Bonnet, F. Court and L. Leibler, *Macromol. Symp.*, 2003, **198**, 309.
13 T. Fine, R. Inoubli, P. Gérard and J. P. Pascault, in *Epoxy Polymers, New Materials and Innovations*, ed. J. P. Pascault and R. J. J. Williams, Wiley-VCH, Weinheim, 2010, p. 289.
14 A. Tercjak, M. Larrañaga, M. D. Martin and I. Mondragon, *J. Therm. Anal. Calorim.*, 2006, **86**(3), 663.
15 B. Nandan, B. K. Kuila and M. Stamm, *Eur. Polym. J.*, 2011, **47**, 584.
16 J. Gutierrez, I. Mondragon and A. Tercjak, *Polymer*, 2011, **52**, 5699.
17 A. Tercjak, J. Gutierrez, M. D. Martin and I. Mondragon, *Eur. Polym. J.*, 2012, **48**, 16.
18 F. Meng, S. Zheng, W. Zhang, H. Li and Q. Liang, *Macromolecules*, 2006, **39**, 711.
19 F. Meng, S. Zheng, H. Li, Q. Liang and T. Liu, *Macromolecules*, 2006, **39**, 5072.
20 H. E. Romeo, I. A. Zucchi, M. Rico, C. E. Hoppe and R. J. J. Williams, *Macromolecules*, 2013, **46**, 4854.
21 R. J. J. Williams, B. A. Rozenberg and J. P. Pascault, *Adv. Polym. Sci.*, 1997, **128**, 95.
22 A. B. Leonardi, I. A. Zucchi and R. J. J. Williams, *Eur. Polym. J.*, 2015, **71**, 164.
23 I. A. Zucchi and W. F. Schroeder, *Polymer*, 2015, **56**, 300.
24 Q. Guo, R. Thomann, W. Gronski, R. Staneva, R. Ivanova and B. Stühn, *Macromolecules*, 2003, **36**, 3635.
25 H. Yi, X. Wang, T. Wei, H. Lin and B. Zheng, *Colloid Polym. Sci.*, 2012, **290**, 1347.
26 C. Zhang, L. Li and S. Zheng, *Macromolecules*, 2013, **46**, 2740.
27 J. J. Crassous, P. Schurtenberger, M. Ballauff and A. M. Mihut, *Polymer*, 2015, **62**, A1.
28 I. E. Dell'Erba and R. J. J. Williams, *Polym. Eng. Sci.*, 2006, **46**, 351.
29 A. Vázquez, D. Bentaleb and R. J. J. Williams, *J. Appl. Polym. Sci.*, 1991, **43**, 967.
30 C. E. Hoppe, M. J. Galante, P. A. Oyanguren and R. J. J. Williams, *Macromolecules*, 2002, **35**, 6324.
31 B. A. Rozenberg, *Adv. Polym. Sci.*, 1986, **75**, 113.
32 A. Vázquez, L. Matějka, P. Spacek and K. Dušek, *J. Polym. Sci., Part A: Polym. Chem.*, 1990, **28**, 2305.
33 I. A. Zucchi, M. J. Galante and R. J. J. Williams, *Polymer*, 2005, **46**, 2603.
34 L. Yin and M. A. Hillmyer, *Macromolecules*, 2011, **44**, 3021.
35 R. A. MacPhail, H. L. Strauss, R. G. Snyder and C. A. Elliger, *J. Phys. Chem.*, 1982, **88**, 334.
36 R. G. Snyder, H. L. Strauss and C. A. Elliger, *J. Phys. Chem.*, 1982, **86**, 5145.
37 A. N. Parikh, S. D. Gillmor, J. D. Beers, K. M. Beardmore, R. W. Cutts and B. I. Swanson, *J. Phys. Chem. B*, 1999, **103**, 2850.

